Surface oxygen-mediated ultrathin PtRuM (Ni, Fe, and Co) nanowires boosting methanol oxidation reaction

Hongdong Li[#], Yue Pan[#], Dan Zhang, Yi Han, Zuochao Wang, Yinnan Qin, Shuangyan Lin, Xueke Wu, Huan Zhao, Jianping Lai, Bolong Huang* and Lei Wang**

H. Li, Y. Pan, D. Zhang, Y. Han, Z. Wang, Y. Qin, X. Wu, H. Zhao, Prof. J. Lai, Prof. L. Wang
Key Laboratory of Eco-chemical Engineering, Taishan scholar advantage and characteristic discipline team of Eco chemical process and technology, College of Chemistry and Molecular Engineering, Qingdao University of Science and Technology, Qingdao 266042, P. R. China
E-mail: jplai@qust.edu.cn, inorchemwl@126.com

Prof. B. Huang
Department of Applied Biology and Chemical Technology, The Hong Kong Polytechnic University, Hung Hom, Kowloon, Hong Kong SAR, China
E-mail: bhuang@polyu.edu.hk

Dr. S. Lin
Key Laboratory for Photonic and Electronic Bandgap Materials, Ministry of Education, School of Physics and Electronic Engineering, Harbin Normal University, Harbin 150025, P. R. China

[#]Equal Contribution

Keywords: ultrathin; oxygen-doped; ternary nanowire; synergetic effect; methanol oxidation

Abstract: Improving the electrocatalytic activity and durability of electrocatalysts is of vital importance to the direct methanol fuel cells. PtRu materials are the most effective catalysts for methanol oxidation reaction (MOR) in acidic medium, but it still exhibits partial defects, including limited catalytic activity and serious CO poisoning. Here we prepared a series of surface-doped ultrathin PtRuM (M = Ni, Fe, and Co) nanowires (NWs) with oxygen (O), termed O-doped PtRuM (PtRuM-O). All these prepared materials show ultrahigh electrocatalytic activity and excellent durability for MOR in acidic medium due to the optimal electronic structures induced by the introduction of electroactive O. Until now, in the reported Pt-based materials article (**Table S1**), the optimal $Pt_{62}Ru_{18}Ni_{20}$-O/C electrocatalyst shows the highest mass activity of 2.72 A mg^{-1}_{pt} for MOR in the acidic medium, which is 1.42, 5.14 and 9 times higher than that of $Pt_{62}Ru_{18}Ni_{20}$/C (1.91 A mg^{-1}_{pt}), $Pt_{65}Ru_{35}$/C (0.47 A mg^{-1}_{pt}) and Pt/C (0.30 A mg^{-1}_{pt}) NWs catalysts, respectively. And the

$Pt_{62}Ru_{18}Ni_{20}$-O/C catalyst still retains 92% of initial mass activity after 1000 cyclic voltammetry (CV). The CO onset potential and peak potential of $Pt_{62}Ru_{18}Ni_{20}$-O/C show a negative shift compare with $Pt_{62}Ru_{18}Ni_{20}$/C, $Pt_{65}Ru_{35}$/C and Pt/C NWs catalysts, indicating that the $Pt_{62}Ru_{18}Ni_{20}$-O/C catalyst has the better CO anti-poisoning. And the prepared electrocatalysts also show better MOR performance in alkaline medium. Density functional theory (DFT) calculations prove that the introduction of O to PtRuNi significantly boosts the MOR performance by strengthening the adsorption of initial CH_3OH induced by the electroactive O-2p bands. Meanwhile, the much larger energy barrier for CO generation indicates the much lower probability of catalyst poisoning of the O-doped PtRuNi.

Direct methanol fuel cells have been extensively investigated due to its environmentally friendly, it can convert chemical energy into other energies with no byproduct.[1-5] For methanol oxidation reaction (MOR) in acidic medium, in order to overcome the defects (CO poisoning, etc.) on Pt catalyst, bimetallic alloy Pt-M (Ru, Au, Ag Ni, Fe, Co, Zn, Ti, Cu, etc.) catalysts have been widely studied.[6-22] Among them, Pt-Ru catalyst is the most effective and has better CO anti-poisoning performance for MOR in acidic medium.[6][23-24] Based on the "bifunctional mechanism", the addition of Ru can cause two effects: firstly, the electrons can transfer from Ru to Pt, weakening the interaction between Pt and CO. Secondly, it may increase oxygen species coverage on the catalyst surface at lower potential.[25-26]

In order to further improve the activity and durability (stability and CO anti-poisoning) of electrocatalysts for MOR, and reduce the amount of precious metals, so it is essential to introduce another metal element (Ni, Fe, Co, Cu, Pd, etc.) to prepare PtRu based ternary alloy nanocatalysts with sundry nanostructures and make significant progress.[27-31] Other Pt-based multi-metal nanocatalysts with different nanostructures have also been extensively utilized for direct methanol fuel cells in acidic medium.[32-36] In addition, the electronic properties of catalysts can be enhanced

by introducing some non-metallic elements (O, N, P, etc.) with the appropriate methods,[37-42] then strengthening the adsorption of reactants and changing the energy barrier in the reaction process, therefore it is an effective strategy to improve the electrocatalytic activity of catalysts. From the view of structure, the nanostructures with ultrathin size (<2 nm) can expose more active sites which can enhance catalytic activity significantly.[1] And one-dimensional (1D) nanowire structures have larger contact areas with support than nanoparticles. It contributes to the bond between the catalysts and the support, thereby increasing the activity and stability.[32] Therefore, to boost MOR performances of catalysts, it is an effective strategy to synthesize the non-metal doped PtRu-based ultrathin ternary metal 1D nanowire catalysts.

In this work, we further explored and enhanced the MOR performance of PtRuM (M= Ni, Fe, and Co) nanocatalysts by adopting the surface engineering strategy. We synthesized a class of ultrathin ternary PtRuM (M= Ni, Fe, and Co) nanowires by a general wet-chemical method. After the nanowires were combined with carbon (C), the products were dried and annealed at 220 °C for 1 h under atmospheric conditions to obtain O-doped PtRuM/C, termed PtRuM-O/C (see the Supporting Information for details). Among all the ultrathin nanowires we synthesized, the $Pt_{62}Ru_{18}Ni_{20}$-O/C electrocatalyst exhibits the best electrocatalytic activity and durability toward methanol oxidation reaction (MOR) in acidic medium. The mass current density of the ultrathin $Pt_{62}Ru_{18}Ni_{20}$-O/C for MOR is 2.72 A mg^{-1}_{Pt} in acidic medium, 1.4, 5.1 and 9.0 times higher than those of the $Pt_{62}Ru_{18}Ni_{20}$/C (1.91 A mg^{-1}_{Pt}), $Pt_{65}Ru_{35}$/C (0.47 A mg^{-1}_{pt}) and Pt/C (0.30 A mg^{-1}_{Pt}) NWs catalyst, respectively. And after 1000 cyclic voltammetry (CV), the $Pt_{62}Ru_{18}Ni_{20}$-O/C catalyst still retains 92% of initial mass activity. CO stripping experiments also confirmed the contribution of O elements to anti-poisoning, significantly lower onset and peak potentials. In a word, the ultrathin PtRuM-O/C catalystw show excellent catalytic activity and durability for MOR in acidic solutions than that of PtRuM/C, PtRu/C and Pt/C NWs catalysts. And from both electronic behaviors and energetic comparison, we have confirmed the MOR performance follows the order: O-doped PtRuNi >

PtRuNi > PtRu. In addition, the O-doped PtRuNi electrocatalyst also demonstrates the superior anti-poisoning capability than simple PtRuNi and PtRu alloys. In brief, these O-doped PtRuM (M=Ni, Fe, Co) nanowires have better performance and CO anti-poisoning and can be used as electrocatalysts for direct alcohol fuel cells.

In a typical preparation of ultrathin ternary PtRuNi NWs, platinum (II) acetylacetonate ($Pt(acac)_2$), ruthenium (III) 2,4-pentanedionate ($Ru(acac)_3$) and nickel (II) acetylacetonate ($Ni(acac)_2$) as metal precursors, (1-Hexadecyl)trimethylammonium chloride (CTAC) as surfactant, glucose and molybdenumhexacarbonyl ($Mo(CO)_6$) as reducing agents were added into oleylamine in a vial. Then the mixture was sonicated for 1 h at room temperature and was heated to 180 °C for 2 h under magnetic stirring. Then the black colloidal products were collected by centrifugation and washed two or three times with an ethanol/cyclohexane mixture and dispersed in cyclohexane. Finally, the O-doped PtRuM (PtRuM-O) nanowires were obtained by annealing at 220 °C for 1 h under atmospheric conditions.

The typical transmission electron microscopy (TEM) (**Figure 1a** and **b**) images display that the $Pt_{62}Ru_{18}Ni_{20}$-O product is dominated with ultrathin one-dimensional (1D) architectures, the diameter of as-prepared $Pt_{62}Ru_{18}Ni_{20}$-O NWs is about 1.51±0.25 nm (**Figure S3a**, Supporting Information). And the high-resolution TEM (HRTEM) (**Figure 1c**) images of $Pt_{62}Ru_{18}Ni_{20}$-O NWs show that the lattice spacing of 0.213 nm and 0.238 nm, corresponding to the fcc Pt (111) facet and the NiO (111) facet,[38] respectively. The powder X-ray diffraction (PXRD) patterns (**Figure 2a** and **S2**, Supporting Information) of the NWs also reveal the typical Pt fcc structure in as-made NWs, the diffraction peaks were broadened due to the ultrathin structure. And because of the introduction of Ru, Ni, Fe, and Co elements in the Pt lattice, the Pt (111) peak location shifts slightly to a higher 2θ.[28] From the TEM-mapping images (**Figure 1d**), we can see that Pt, Ru, Ni, and O elements are uniformly distributed within the NWs, confirmed that the formation of the O-doped ternary metal nanostructures. By adjusting the molar ratio of $Ru(acac)_3$ and $Ni(acac)_2$, similar ultrathin NWs with

different atomic ratios were also prepared (**Figure S1a** and **b**, Supporting Information). The Pt NWs (**Figure S1d,** Supporting Information), PtRu NWs (**Figure S1c**, Supporting Information), PtRuFe NWs (**Figure 1e**) and PtRuCo NWs (**Figure 1f**) also were synthesized by the oil phase method (see the Supporting Information for details). The composition of the prepared nanowires was determined by inductively coupled plasma atomic emission spectroscopy (ICP-AES), they were $Pt_{65}Ru_{35}$, $Pt_{62}Ru_{18}Ni_{20}$, $Pt_{61}Ru_{25}Ni_{14}$, $Pt_{58}Ru_{14}Ni_{28}$, $Pt_{61}Ru_{16}Fe_{23}$, and $Pt_{59}Ru_{19}Co_{22}$, respectively, which were in good agreement with those measured by TEM-EDS (**Figure S3d-f** and **Figure S4**, Supporting Information).

To understand the enhancement effect of the catalysts for MOR clearly, the XPS measurement of electrocatalysts were executed. The Pt 4f XPS spectra (**Figure 2b**) of $Pt_{62}Ru_{18}Ni_{20}$-O NWs, $Pt_{62}Ru_{18}Ni_{20}$ NWs, and $Pt_{65}Ru_{35}$ NWs shows that the Pt 4f binding energies are all negative shift compared to the Pt NWs. The $Pt_{62}Ru_{18}Ni_{20}$-O NWs and $Pt_{62}Ru_{18}Ni_{20}$ NWs show the maximum negative change of about 0.35 eV. It is indicated that the electron transfer from Ru to Pt because of the higher electronegativity of Pt, weakening the interaction between Pt and CO and promoting the MOR.[25,26][43] From the Pt 4f XPS spectra of $Pt_{62}Ru_{18}Ni_{20}$-O NWs and $Pt_{62}Ru_{18}Ni_{20}$ NWs, the Pt^{2+} and Pt^{4+} oxidation states can be more clearly observed in $Pt_{62}Ru_{18}Ni_{20}$-O NWs than $Pt_{62}Ru_{18}Ni_{20}$ NWs. According to the Ni XPS spectra (**Figure 2c**), there is more NiO and less $Ni(OH)_2$ states existed in $Pt_{62}Ru_{18}Ni_{20}$-O NWs than $Pt_{62}Ru_{18}Ni_{20}$ NWs due to the dehydration of $Ni(OH)_2$ during annealing, it is confirmed that the oxidation of Ni.[38] It confirms that the O elements were successfully introduced into the prepared materials and the electroactive O is useful for methanol electrooxidation.

All the prepared nanocatalysts toward methanol electrooxidation performance were examined in acidic solutions by cyclic voltammetry (CV). Before the measurements, Pt NWs, $Pt_{65}Ru_{35}$ NWs, $Pt_{62}Ru_{18}Ni_{20}$ NWs, $Pt_{61}Ru_{25}Ni_{14}$ NWs, and $Pt_{58}Ru_{14}Ni_{28}$ NWs were loading on the Ketjen Black-300 as catalysts, and then thermal annealing to remove the surfactant around NWs. The final products

were denoted as Pt/C, $Pt_{65}Ru_{35}$/C, $Pt_{62}Ru_{18}Ni_{20}$-O/C, $Pt_{61}Ru_{25}Ni_{14}$-O/C, and $Pt_{58}Ru_{14}Ni_{28}$-O/C, respectively (**Figure S10-S13**, Supporting Information). **Figure 3a** shows the CV curves of Pt/C, $Pt_{65}Ru_{35}$/C, $Pt_{62}Ru_{18}Ni_{20}$-O/C, $Pt_{61}Ru_{25}Ni_{14}$-O/C and $Pt_{58}Ru_{14}Ni_{28}$-O/C in N_2-saturated 0.5 M H_2SO_4 at a scan rate of 20 mV S^{-1}. From **Figure 3a**, the specific electrochemically active surface areas (ECSA) of $Pt_{62}Ru_{18}Ni_{20}$-O/C, $Pt_{61}Ru_{25}Ni_{14}$-O/C, $Pt_{58}Ru_{14}Ni_{28}$-O/C, and $Pt_{65}Ru_{35}$/C electrocatalysts are determined to be 55.5 $m^2\ g^{-1}$, 52.2 $m^2\ g^{-1}$, 49.8 $m^2\ g^{-1}$, and 45.4 $m^2\ g^{-1}$, respectively, which are higher than that of the Pt/C catalyst (40.3 $m^2\ g^{-1}$).

As shown in **Figure 3b**, the ultrathin $Pt_{62}Ru_{18}Ni_{20}$-O/C catalyst exhibits the best activity for MOR in 0.5 M H_2SO_4 and 0.5 M CH_3OH electrolyte at a sweep rate of 20 mV s^{-1}. And the $Pt_{62}Ru_{18}Ni_{20}$-O/C achieves 9.0 times higher in mass activity (2.72 A mg^{-1}_{pt}) and 2.8 times higher in specific activity (4.36 mA cm^{-2}) than that of Pt/C NWs catalysts (0.30 A mg^{-1}_{pt}, 1.56 mA cm^{-2}) for MOR in acidic medium. Other catalysts $Pt_{61}Ru_{25}Ni_{14}$-O/C, $Pt_{58}Ru_{14}Ni_{28}$-O/C, and $Pt_{65}Ru_{35}$/C showed lower activities with values of 2.23 A mg^{-1}_{pt}, 1.20 A mg^{-1}_{pt} and 0.47 A mg^{-1}_{pt} (**Figure 3c**), respectively. Moreover, the $Pt_{62}Ru_{18}Ni_{20}$-O/C showed better MOR activity than $Pt_{62}Ru_{18}Ni_{20}$/C (**Figure 3e**), it is 1.42 times higher than $Pt_{62}Ru_{18}Ni_{20}$/C (1.91 A mg^{-1}_{pt}). And the $Pt_{62}Ru_{18}Ni_{20}$-O/C also displays the best mass activity in recently reported Pt-based materials in acidic medium (**Table S1**, Supporting Information). The I_f/I_b ratio represents the CO tolerance of electrocatalysts. As shown in **Table S2**, the I_f/I_b ratio of $Pt_{62}Ru_{18}Ni_{20}$-O/C catalyst is 1.47, which is larger than those of $Pt_{62}Ru_{18}Ni_{20}$/C (1.26), $Pt_{65}Ru_{35}$/C (1.45) and Pt/C catalysts (0.96), this also indicates that the $Pt_{62}Ru_{18}Ni_{20}$-O/C catalyst has better performance of MOR and strong CO anti-poisoning.

For studying the stability of the ultrathin PtRuM/C in methanol electrooxidation reaction, the long term current-time (I−t) was tested at 0.7 V *vs.* RHE. As shown in **Figure 3d**, during the whole test, the current density of the ultrathin $Pt_{62}Ru_{18}Ni_{20}$-O/C (334 mA mg^{-1}_{pt}) is still higher than that of $Pt_{65}Ru_{35}$/C (44 mA mg^{-1}_{pt}) and Pt/C (0.34 mA mg^{-1}_{pt}) NWs nanocatalysts after 5000 s. From **Figure 3f**, the $Pt_{62}Ru_{18}Ni_{20}$-O/C catalyst has higher stability than the $Pt_{62}Ru_{18}Ni_{20}$/C. And the durability of

the PtRuM/C catalysts were also examined by 1000 cycles in 0.5 M H_2SO_4, the mass activity of the $Pt_{62}Ru_{18}Ni_{20}$-O/C, $Pt_{62}Ru_{18}Ni_{20}$/C, $Pt_{65}Ru_{35}$/C and Pt/C NWs catalysts decayed by about of 7.6%, 18.3%, 19.6% and 20.2%, respectively, further confirming the superior stability of $Pt_{62}Ru_{18}Ni_{20}$-O/C nanocatalyst (**Figures S21**, Supporting Information). Besides, no significant morphology changes were noticed in $Pt_{62}Ru_{18}Ni_{20}$-O/C (**Figure S10a and b**, Supporting Information). The XRD of $Pt_{62}Ru_{18}Ni_{20}$-O/C before and after reaction was also measured (**Figure S14**, Supporting Information), it is indicated that the structure of the catalyst is stable because the typical peak are well maintained.

And then the MOR activity of the PtRuNi NWs in alkaline (1 M KOH +1 M CH_3OH) was also examined. In **Figure S16b** and **c**, the $Pt_{62}Ru_{18}Ni_{20}$-O/C also exhibits the best activity for MOR, it achieves 1.17, 1.98, 3.81 times higher in mass activity (5.03 A mg^{-1}_{pt}) for MOR than $Pt_{62}Ru_{18}Ni_{20}$/C (4.30 A mg^{-1}_{pt}), $Pt_{65}Ru_{35}$/C (2.54 A mg^{-1}_{pt}) and Pt/C (1.32 A mg^{-1}_{pt}) NWs catalysts, respectively. And the $Pt_{62}Ru_{18}Ni_{20}$-O/C shows the better mass activity in alkaline medium among recently Pt-based electrocatalysts (**Table S3**, Supporting Information). According to the I_f/I_b ratio (**Table S4**, Supporting Information), the $Pt_{62}Ru_{18}Ni_{20}$-O/C catalyst (2.43) has excellent anti-poisoning performance than those of $Pt_{62}Ru_{18}Ni_{20}$/C (2.30), $Pt_{65}Ru_{35}$/C (1.98) and Pt/C (1.74) NWs catalysts. Additionally, chronoamperometric tests measure the stability of the catalysts for MOR at 0.7 V *vs.* RHE. From the **Figure S16d** and **f**, the $Pt_{62}Ru_{18}Ni_{20}$-O/C also shows the best stability among all prepared electrocatalysts in alkaline solution, the current density of $Pt_{62}Ru_{18}Ni_{20}$-O/C remain 980 mA mg^{-1}_{pt} for MOR, it is 1.17-fold, 3.05-fold and 5.38-fold than those of $Pt_{62}Ru_{18}Ni_{20}$/C (840 mA mg^{-1}_{pt}), $Pt_{65}Ru_{35}$/C (321 mA mg^{-1}_{pt}) and Pt/C (182 mA mg^{-1}_{pt}) NWs catalysts, respectively.

The CO stripping experiments were performed for further knowing the durability of all electrocatalysts. In acidic medium, compared with that of Pt/C (0.795 V *vs.* RHE) NWs catalyst, the peak potentials of the $Pt_{65}Ru_{35}$/C (0.713 V *vs.* RHE), $Pt_{62}Ru_{18}Ni_{20}$/C (0.655 V *vs.* RHE) and $Pt_{62}Ru_{18}Ni_{20}$-O/C (0.626 V *vs.* RHE) all shift negatively, showing better CO anti-poisoning performance (**Figure 4**). More importantly, the $Pt_{62}Ru_{18}Ni_{20}$-O/C exhibits a higher CO resistance by

O-doped, leading to 29 mV negative shift compared to that for $Pt_{62}Ru_{18}Ni_{20}$/C. Compared with other catalysts (PtRuNi-O/C with different rations and PtRuM (Fe, Co)-O/C, **Figure 4b**), the $Pt_{62}Ru_{18}Ni_{20}$-O/C also has the lowest onset potential and peak potential. In alkaline solution, the CO onset potential of $Pt_{62}Ru_{18}Ni_{20}$-O/C, $Pt_{62}Ru_{18}Ni_{20}$/C, $Pt_{65}Ru_{35}$/C, and Pt/C NWs catalysts are 0.41 V, 0.44 V, 0.45 V and 0.55 V *vs.* RHE, respectively (**Figure S17** and **S18a** and **b**, Supporting Information). In all prepared catalysts, the $Pt_{62}Ru_{18}Ni_{20}$-O/C exhibits the highest CO resistance in acidic or alkaline mediums. Therefore, the enhancement of the activity and durability of $Pt_{62}Ru_{18}Ni_{20}$-O/C catalysts are attributed to the introduction of electroactive O and the stable structure.

To illustrate the superior MOR performance and anti-poisoning capability of O-doped PtRuNi, we utilized DFT calculations to reveal the electronic and energetic advantages over the PtRu and PtRuNi. From the PtRu, the electronic bonding and anti-bonding distribution are highly ordered on the surface, in which the electroactive region focused on the Ru sites (**Figure 5a**). When Ni is introduced to the alloy, an evident interruption of the electronic distribution is noted. Both Ni and Ru sites are electroactive (**Figure 5b**). For O-doped PtRuNi, the electronic distribution has been reconstructed, in which the surface electroactive region is relocated to the O sites. Such surface modification is of significance in determining MOR performance (**Figure 5c**). Then we further investigated the projected partial density of states for PtRu, PtRuNi, and O-doped PtRuNi to reveal the electronic contributions. For the simple PtRu alloys, Ru-4d bands occupy a higher position at 0.75 eV below the Fermi level (EF). Meanwhile, Pt sites located at a much lower position at Ev-3.0 eV (Ev denotes to 0 eV) (**Figure 5d**). When Ni is introduced to PtRu, Ni-3d bands and Ru-4d bands locate similar positions, leading to a suppressed electroactivity of Ru for the electron transfer. The Pt-5d bands are still pinned near the Ev-3.0 eV (**Figure 5e**). In O-doped PtRuNi, both Ni-3d bands and Pt-5d bands are substantially suppressed to lower positions at Ev-1.75 eV and Ev-3.80 eV, respectively. O-2p bands cover a broad range and even cross the Fermi level, indicating a high electroactivity and oxidation ability for efficient MOR (**Figure 5f**). For the initial reactant CH_3OH,

only O-doped PtRuNi shows the strongest overlap probability, especially the Ni, Ru, and O sites, supporting the tight adsorption with efficient electron transfer between adsorbates and catalyst surfaces. In comparison, both PtRu and PtRuNi display very limited overlap with s,p bands of CH_3OH (**Figure 5g**). The key adsorbates in determining the MOR and anti-poisoning performance also support the stability of the O-doped PtRuNi catalyst (**Figure 5h**).

From the energetic perspective, both the MOR process and the CO poisoning process are demonstrated on PtRu, PtRuNi, and O-doped PtRuNi catalysts. For the MOR process, all three catalysts show the overall exothermal reactions, in which the largest energy releasement of -4.65 eV is noted for O-doped PtRuNi. Most of the MOR steps show the downhill physicochemical trend. However, all three catalysts exhibit the largest energetic barrier at the final dehydrogenation from [*COOH] to form CO_2. Notably, the energy barrier in O-doped PtRuNi has been largely reduced to 0.49 eV when compared to 1.56 eV, 1.08 eV for PtRu and PtRuNi, respectively. Thus, O-doped PtRuNi shows the most energetically favorable physicochemical trend for MOR process, supporting the experiment results (**Figure 5i**). On the other side, we also notice two continuous energy barriers of the 1.11 eV and 0.74 eV of O-doped PtRuNi for the catalyst poisoning process, which is much larger than the energy barrier in MOR process. This demonstrates the suppression of the catalyst poisoning process. Meanwhile, the energy barrier in catalyst poisoning for PtRu and PtRuNi is only 0.06 and 0.36 eV, which are much smaller than the energy barriers in MOR. The much larger energy releasement also indicates that the high catalyst poisoning probability during MOR process for PtRu and PtRuNi (**Figure 5j**). Thus, we confirm the remarkable performance of O-doped PtRuNi in the MOR and anti-poisoning based on the optimal electronic structures induced by the introduction of electroactive O.

Meanwhile, the MOR performances of PtRuFe NWs and PtRuCo NWs were also investigated in acidic and alkaline solutions. In 0.5 M H_2SO_4 and 0.5 M methanol solution, both $Pt_{61}Ru_{16}Fe_{23}$-O/C and $Pt_{59}Ru_{19}Co_{22}$-O/C (**Figure S19a** and **b**, Supporting Information) display better MOR

performance than $Pt_{61}Ru_{16}Fe_{23}$/C and $Pt_{59}Ru_{19}Co_{22}$/C. At a fixed potential of 0.8 V *vs.* RHE, the mass activities of $Pt_{61}Ru_{16}Fe_{23}$-O/C and $Pt_{59}Ru_{19}Co_{22}$-O/C are 2.15 A mg^{-1}_{pt} and 2.06 A mg^{-1}_{pt}, about 1.09 and 1.36 times higher than that of $Pt_{61}Ru_{16}Fe_{23}$/C (1.58 A mg^{-1}_{pt}) and $Pt_{59}Ru_{19}Co_{22}$/C (1.51 A mg^{-1}_{pt}), respectively. The I_f/I_b ratio of $Pt_{61}Ru_{16}Fe_{23}$-O/C and $Pt_{59}Ru_{19}Co_{22}$-O/C for MOR is 1.33 and 1.51, respectively. Through the CO stripping experiment (**Figure 4b**), I-t test (**Figure S19c** and **d**, Supporting Information) and 1000 CV cycles (**Figure S21**, Supporting Information), it reveals that $Pt_{61}Ru_{16}Fe_{23}$-O/C and $Pt_{59}Ru_{19}Co_{22}$-O/C electrocatalysts have also the enhanced durability compare with $Pt_{61}Ru_{16}Fe_{23}$/C, $Pt_{59}Ru_{19}Co_{22}$/C, and Pt/C NWs catalysts.

In conclusion, we synthesized a series of O-doped ultrathin PtRuM (M = Ni, Fe, and Co) NWs with strong durability and activity for methanol oxidation in acidic medium and alkaline medium. Because of the electron effects and the presence of oxidation states in metals, $Pt_{62}Ru_{18}Ni_{20}$-O/C exhibited the notable mass activity (2.72 A mg^{-1}_{pt}) and durability (maintain 92% of mass activity after 1000 CVs), the higher ration of I_f/I_b and CO anti-poisoning for MOR compare with $Pt_{62}Ru_{18}Ni_{20}$/C and Pt/C NWs nanocatalysts in acidic electrolyte. Similarly, the prepared PtRuM-O/C catalysts also show better performance of MOR and stability in alkaline medium. From theoretical calculations, the systematic comparison of the electronic behaviors and energetic reaction trend shows that the enhanced electroactivity towards the MOR process induced by the O dopants in PtRuNi. The CO generation is much less energetic favorable than the MOR, confirming the substantially strengthened anti-poisoning capability in the O-doped PtRuNi. The design strategy of using the non-metallic elements and transition metal elements to synergistically adjust the electronic structure of bi-functional metal catalysts may be extended to other electrocatalysis field.

Supporting Information

Supporting Information is available from the Wiley Online Library or from the author.

Acknowledgements
This work was supported by the National Natural Science Foundation of China (21571112, 51572136, 51772162, 51802171), the Taishan Scholars program, Natural Science Foundation of Shandong Province, China (ZR2018BB031), Open Fund of the Key Laboratory of Eco-chemical Engineering (Qingdao University of Science and Technology, No. KF1702).

Received: ((will be filled in by the editorial staff))
Revised: ((will be filled in by the editorial staff))
Published online: ((will be filled in by the editorial staff))

References

[1] M. A. Zeb Gul Sial, M. A. Ud Din, X. Wang, *Chem. Soc. Rev.* **2018**, *47*, 6175.

[2] Y. Feng, H. Liu, J. Yang, *Sci. Adv.* **2017**, *3*, e1700580.

[3] A. Chen, P. Holt-Hindle, *Chem. Rev.* **2010**, *110*, 3767.

[4] C. Bianchini, P. K. Shen, *Chem. Rev.* **2009**, *109*, 4183.

[5] Z. Xia, X. Zhang, H. Sun, S. Wang, G. Sun, *Nano Energy* **2019**, *65*, 104048.

[6] W.-Y. Zhao, B. Ni, Q. Yuan, P.-L. He, Y. Gong, L. Gu, X. Wang, *Adv. Energy Mater.* **2017**, *7*, 1601593.

[7] X. Zhang, I. G. A. Ossufo, H. Ye, Y. Huang, S. Ge, Z. Xiang, Y. Cui, R. Wang, *ChemCatChem* **2019**, *DOI: 10.1002/cctc.201900649.*

[8] J. Zhang, H. Li, J. Ye, Z. Cao, J. Chen, Q. Kuang, J. Zheng, Z. Xie, *Nano Energy* **2019**, *61*, 397.

[9] P. Yang, X. Yuan, H. Hu, Y. Liu, H. Zheng, D. Yang, L. Chen, M. Cao, Y. Xu, Y. Min, Y. Li, Q. Zhang, *Adv. Funct. Mater.* **2017**, *28*, 1704774.

[10] H. Yang, J. Zhang, K. Sun, S. Zou, J. Fang, *Angew. Chem. Int. Ed.* **2010**, *49*, 6848.

[11] Y. Yamauchi, A. Tonegawa, M. Komatsu, H. Wang, L. Wang, Y. Nemoto, N. Suzuki, K. Kuroda, *J. Am. Chem. Soc.* **2012**, *134*, 5100.

[12] X. Xu, X. Zhang, H. Sun, Y. Yang, X. Dai, J. Gao, X. Li, P. Zhang, H.-H. Wang, N.-F. Yu, S.-G. Sun, *Angew. Chem. Int. Ed.* **2014**, *53*, 12522.

[13] D. Xu, Z. Liu, H. Yang, Q. Liu, J. Zhang, J. Fang, S. Zou, K. Sun, *Angew. Chem. Int. Ed.* **2009**, *48*, 4217.

[14] B. Y. Xia, H. B. Wu, X. Wang, X. W. Lou, *J. Am. Chem. Soc.* **2012**, *134*, 13934.

[15] B. Y. Xia, H. B. Wu, N. Li, Y. Yan, X. W. Lou, X. Wang, *Angew. Chem. Int. Ed.* **2015**, *54*, 3797.

[16] B. Wu, D. Hu, Y. Kuang, B. Liu, X. Zhang, J. Chen, *Angew. Chem. Int. Ed.* **2009**, *48*, 4751.

[17] J. Suntivich, Z. Xu, C. E. Carlton, J. Kim, B. Han, S. W. Lee, N. Bonnet, N. Marzari, L. F. Allard, H. A. Gasteiger, K. Hamad-Schifferli, Y. Shao-Horn, *J. Am. Chem. Soc.* **2013**, *135*, 7985.

[18] Z. Qi, C. Xiao, C. Liu, T. W. Goh, L. Zhou, R. Maligal-Ganesh, Y. Pei, X. Li, L. A. Curtiss, W. Huang, *J. Am. Chem. Soc.* **2017**, *139*, 4762.

[19] J. Lai, L. Zhang, W. Qi, J. Zhao, M. Xu, W. Gao, G. Xu, *ChemCatChem* **2014**, *6*, 2253.

[20] A. Glüsen, F. Dionigi, P. Paciok, M. Heggen, M. Müller, L. Gan, P. Strasser, R. E. Dunin-Borkowski, D. Stolten, *ACS Catal.* **2019**, *9*, 3764.

[21] Z. Cui, H. Chen, M. Zhao, D. Marshall, Y. Yu, H. Abruña, F. J. DiSalvo, *J. Am. Chem. Soc.* **2014**, *136*, 10206.

[22] Q. Shao, P. Wang, X. Huang, *Adv. Funct. Mater.* **2018**, *29*, 1806419.

[23] D.-J. Chen, Y. J. Tong, *Angew. Chem. Int. Ed.* **2015**, *54*, 9394.

[24] E. A. Franceschini, M. M. Bruno, F. J. Williams, F. A. Viva, H. R. Corti, *ACS Appl. Mater. Interfaces* **2013**, *5*, 10437.

[25] M. Watanabe, S. Motoo, *J. Electroanal. Chem.* **1975**, *60*, 275.

[26] M. Watanabe, S. Motoo, *J. Electroanal. Chem.* **1975**, *60*, 267.

[27] H. Wang, Y. Wu, X. Luo, L. Jiao, X. Wei, W. Gu, D. Du, Y. Lin, C. Zhu, *Nanoscale* **2019**, *11*, 10575.

[28] M. E. Scofield, C. Koenigsmann, L. Wang, H. Liu, S. S. Wong, *Energy Environ. Sci.* **2015**, *8*, 350.

[29] Q. Li, X. Wen, G. Wu, H. T. Chung, R. Gao, P. Zelenay, *Angew. Chem. Int. Ed.* **2015**, *54*, 7524.

[30] K. Eid, Y. H. Ahmad, H. Yu, Y. Li, X. Li, S. Y. AlQaradawi, H. Wang, L. Wang, *Nanoscale* **2017**, *9*, 18881.

[31] Z. Cai, Y. Kuang, X. Qi, P. Wang, Y. Zhang, Z. Zhang, X. Sun, *J. Mater. Chem. A* **2015**, *3*, 1182.

[32] W. Zhang, Y. Yang, B. Huang, F. Lv, K. Wang, N. Li, M. Luo, Y. Chao, Y. Li, Y. Sun, Z. Xu, Y. Qin, W. Yang, J. Zhou, Y. Du, D. Su, S. Guo, *Adv. Mater.* **2019**, *31*, 1805833.

[33] K. Wang, H. Du, R. Sriphathoorat, P. K. Shen, *Adv. Mater.* **2018**, *30*, 1804074.

[34] H.-H. Li, S. Zhao, M. Gong, C.-H. Cui, D. He, H.-W. Liang, L. Wu, S.-H. Yu, *Angew. Chem. Int. Ed.* **2013**, *52*, 7472.

[35] J. Huang, Y. Liu, M. Xu, C. Wan, H. Liu, M. Li, Z. Huang, X. Duan, X. Pan, Y. Huang, *Nano Lett.* **2019**, *19*, 5431.

[36] S. Guo, S. Zhang, X. Sun, S. Sun, *J. Am. Chem. Soc.* **2011**, *133*, 15354.

[37] Y. Xie, J. Cai, Y. Wu, Y. Zang, X. Zheng, J. Ye, P. Cui, S. Niu, Y. Liu, J. Zhu, X. Liu, G. Wang, Y. Qian, *Adv. Mater.* **2019**, *31*, 1807780.

[38] Z. Zhao, H. Liu, W. Gao, W. Xue, Z. Liu, J. Huang, X. Pan, Y. Huang, *J. Am. Chem. Soc.* **2018**, *140*, 9046.

[39] X. Huang, Z. Zhao, L. Cao, Y. Chen, E. Zhu, Z. Lin, M. Li, A. Yan, A. Zettl, Y. M. Wang, X. Duan, T. Mueller, Y. Huang, *Science* **2015**, *348*, 1230.

[40] S. Zhao, H. Yin, L. Du, G. Yin, Z. Tang, S. Liu, *J. Mater. Chem. A* **2014**, *2*, 3719.

[41] Y. Meng, X. Zou, X. Huang, A. Goswami, Z. Liu, T. Asefa, *Adv. Mater.* **2014**, *26*, 6510.

[42] L.-X. Ding, A.-L. Wang, G.-R. Li, Z.-Q. Liu, W.-X. Zhao, C.-Y. Su, Y.-X. Tong, *J. Am. Chem. Soc.* **2012**, *134*, 5730.

[43] S.-Y. Ma, H.-H. Li, B.-C. Hu, X. Cheng, Q.-Q. Fu, S.-H. Yu, *J. Am. Chem. Soc.* **2017**, *139*, 5890.

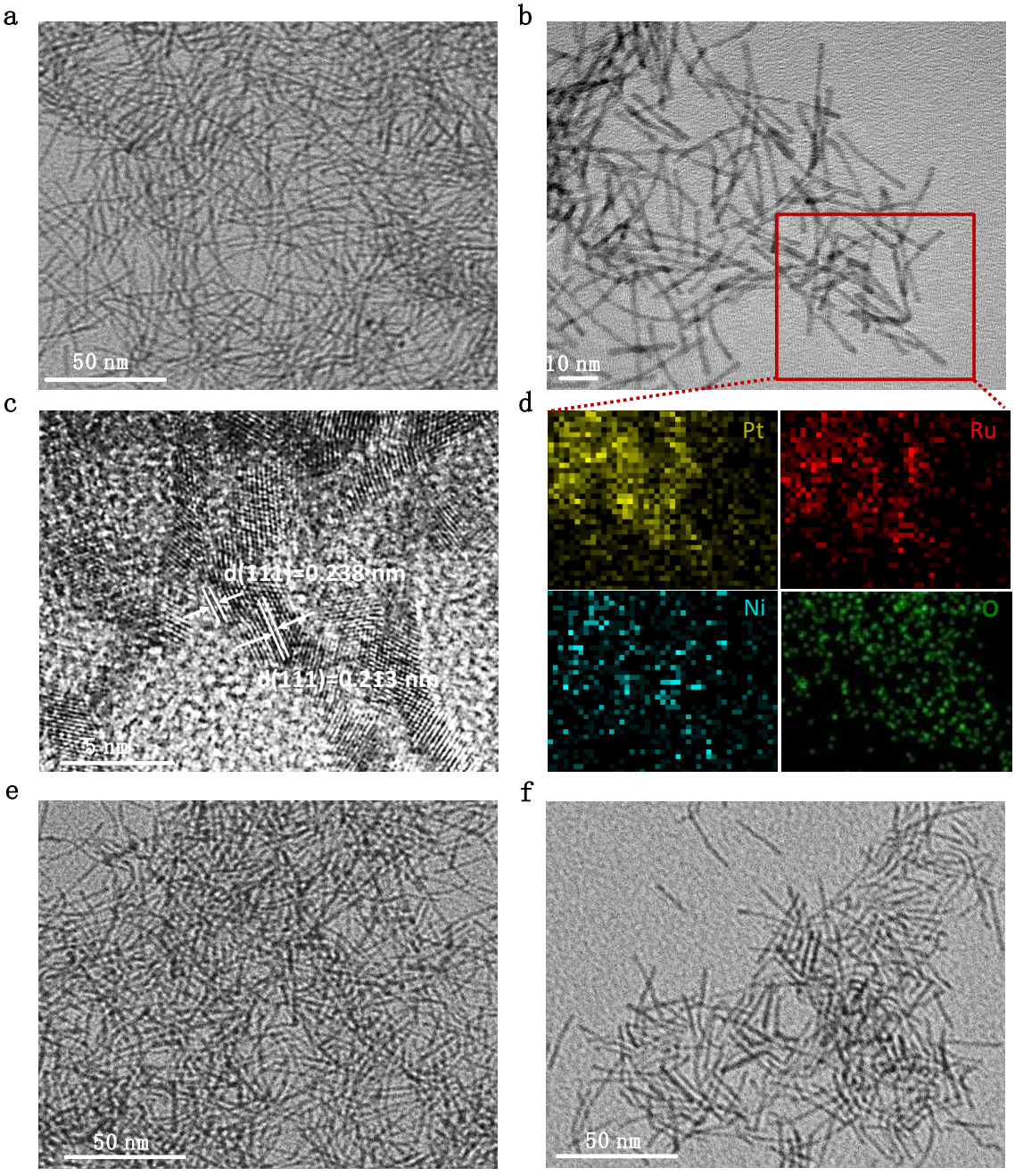

Figure 1. (a, b) TEM and (c) HRTEM images of ultrathin $Pt_{62}Ru_{18}Ni_{20}$-O NWs. (d) The corresponding EDX elemental mapping of the ultrathin $Pt_{62}Ru_{18}Ni_{20}$-O NWs. TEM images of ultrathin (e) $Pt_{61}Ru_{16}Fe_{23}$-O and (f) $Pt_{59}Ru_{19}Co_{22}$-O NWs.

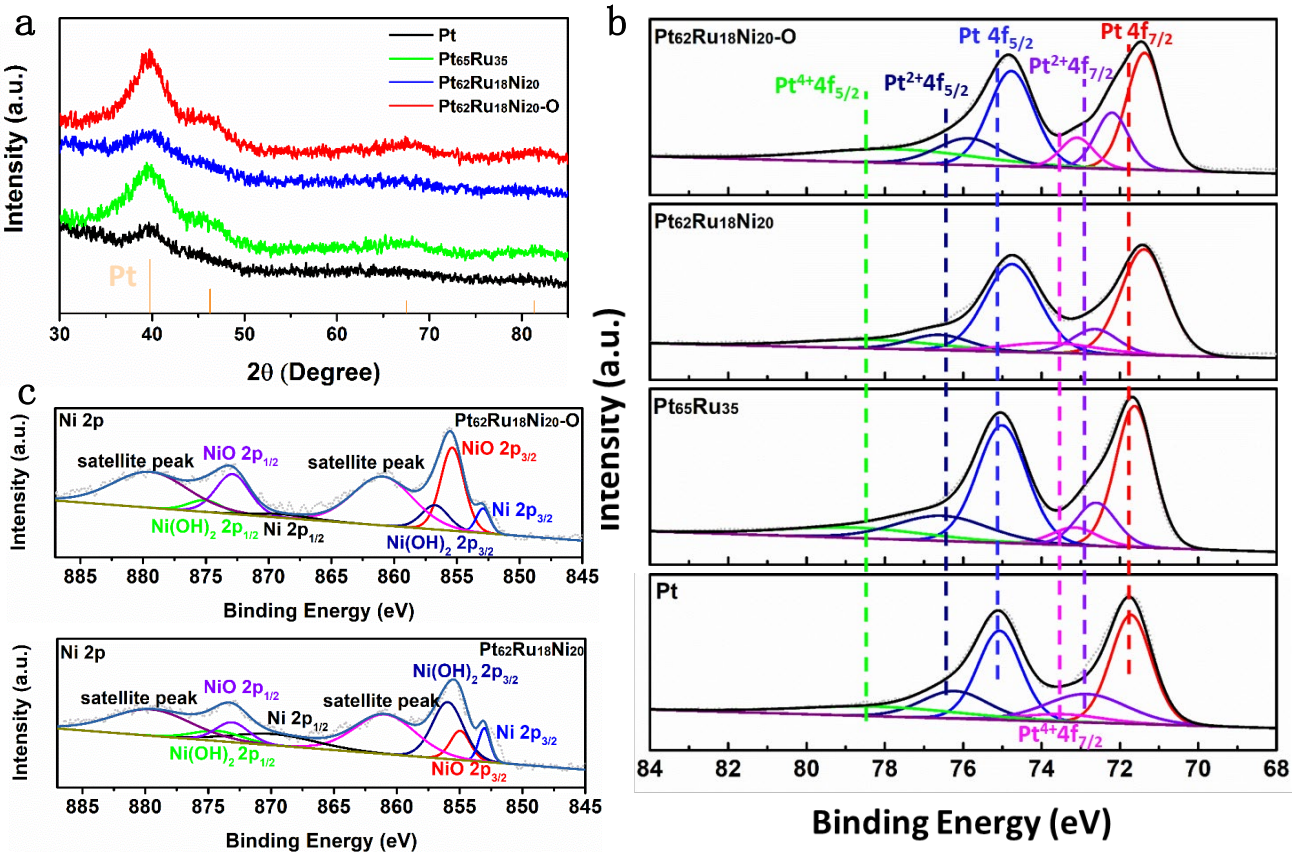

Figure 2. (a) XRD patterns of $Pt_{62}Ru_{18}Ni_{20}$-O NWs, $Pt_{62}Ru_{18}Ni_{20}$ NWs, $Pt_{65}Ru_{35}$ NWs and Pt NWs. (b) Pt 4f XPS spectras of different electrocatalysts. (c) Ni 2p XPS spectras of $Pt_{62}Ru_{18}Ni_{20}$-O NWs and $Pt_{62}Ru_{18}Ni_{20}$ NWs.

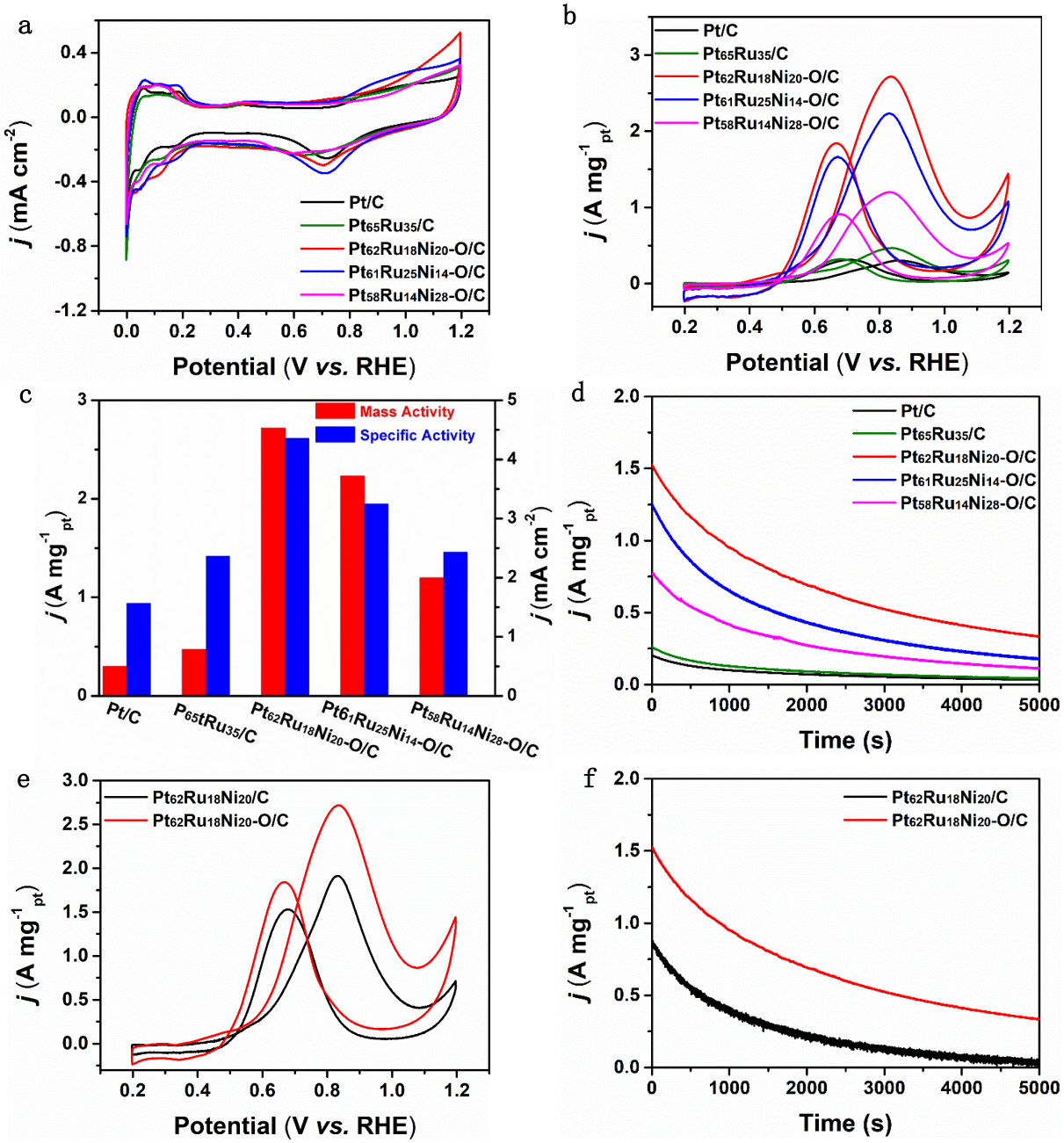

Figure 3. Methanol electro-oxidation performance of different electrocatalysts. (a) CVs in 0.5 M H_2SO_4, (b) CVs for MOR in 0.5 M H_2SO_4 + 0.5 M methanol solution, (c) Corresponding histogram of mass and specific activities, (d) chronoamperometric tests for MOR in 0.5 M H_2SO_4 + 0.5 M methanol solution at 0.7 V *vs.* RHE. (e) CVs, and (f) chronoamperometric tests of $Pt_{62}Ru_{18}Ni_{20}$-O/C and $Pt_{62}Ru_{18}Ni_{20}$/C in 0.5 M H_2SO_4 + 0.5 M methanol solution at 0.7 V *vs.* RHE.

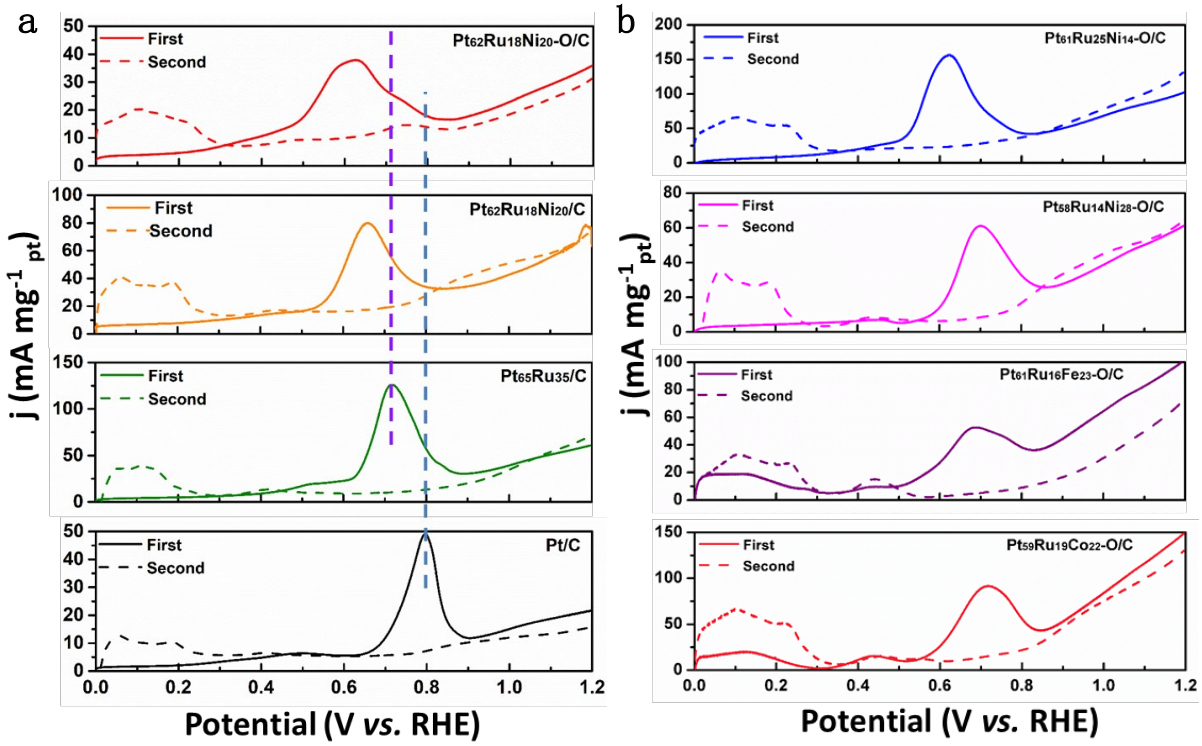

Figure 4. CO stripping curves of different electrocatalysts in 0.5 M H_2SO_4 electrolyte.

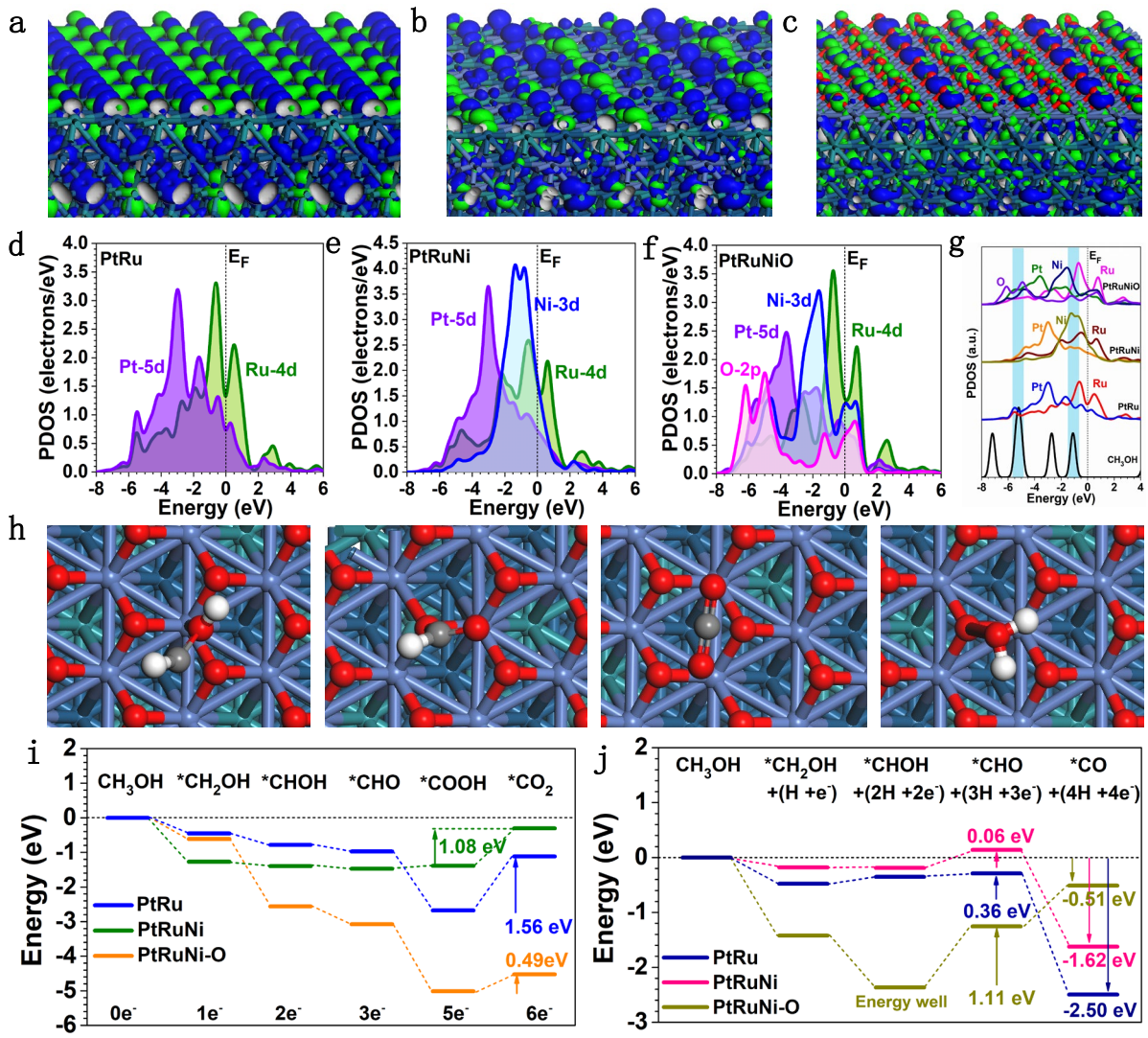

Figure 5. Bonding and anti-bonding orbital distributions for (a) PtRu, (b) PtRuNi and (c) O-doped PtRuNi. The PDOS of (d) PtRu, (e) PtRuNi and (f) O-doped PtRuNi. (g) The PDOS comparison of key adsorbates CH_3OH on PtRu, PtRuNi, and O-doped PtRuNi. (h) The structural configuration of key adsorbates. (i) Energy diagram of the MOR of PtRu, PtRuNi and O-doped PtRuNi. (j) Energy diagram of the catalyst poisoning process of PtRu, PtRuNi and O-doped PtRuNi.

The table of contents entry

A class of oxygen-doped PtRuM nanowires (PtRuM-O/C) are designed and synthesized via a simple method. The optimal $Pt_{62}Ru_{18}Ni_{20}$-O/C catalysts exhibit the highest mass activity, excellent stability and CO anti-poisoning for methanol oxidation reaction in acidic medium.

Keyword: ultrathin; oxygen-doped; ternary nanowire; synergetic effect; methanol oxidation

Hongdong Li[#], Yue Pan[#], Dan Zhang, Yi Han, Zuochao Wang, Yinnan Qin, Shuangyan Lin, Xueke Wu, Huan Zhao, Jianping Lai*, Bolong Huang* and Lei Wang*

Surface oxygen-mediated ultrathin PtRuM (Ni, Fe, and Co) nanowires boosting methanol oxidation reaction